Applied Catalysis B: Environmental 314 (2022) 121499

Contents lists available at ScienceDirect

Applied Catalysis B: Environmental

journal homepage: www.elsevier.com/locate/apcatb

Small-molecule catalyzed H_2O_2 production via a phase-transfer photocatalytic process

Yu Zhao [b,1], Xinke Li [a,1], Xing Fan [a], Hongshuai Wang [a], Yunliang Liu [c], Yuanyuan Chen [a], Tianyu Yang [a], Jing Ye [a], Hui Huang [a], Haitao Li [d], Xiaohong Zhang [a], Yang Liu [a], Haiping Lin [e,*], Yu Zhao [a,*], Zhenhui Kang [a,c,**]

[a] Institute of Functional Nano & Soft Materials (FUNSOM), Jiangsu Key Laboratory for Carbon-Based Functional Materials & Devices, Soochow University, 199 Ren'ai Road, Suzhou 215123, Jiangsu, China
[b] Department of Information Technology, Suzhou Institute of Trade & Commerce, 287 Xuefu Road, Suzhou 215009, Jiangsu, China
[c] Macao Institute of Materials Science and Engineering (MIMSE), MUST-SUDA Joint Research Center for Advanced Functional Materials, Macau University of Science and Technology, Taipa 999078, Macao
[d] Institute for Energy Research, School of Chemistry and Chemical Engineering, Jiangsu University, Zhenjiang 212013, China
[e] School of Physics and Information Technology, Shaanxi Normal University, Xi'an 710062, China

ARTICLE INFO

Keywords:
Hydrogen peroxide
Small-molecule catalyst
Photocatalytic phase-transfer
Transient photovoltage

ABSTRACT

Hydrogen peroxide (H_2O_2) production has long been one of the key technologies in modern chemical industries. Conventional methods for large-scale H_2O_2 production are challenged by either high-energy-consumption or harsh reaction conditions. Here, we demonstrate a strategy to produce H_2O_2 with high yield catalyzed by organophotocatalyst using only H_2O and O_2 as the raw material without the assistance of additional scavengers. Our strategy features the design principle of the organophotocatalyst and a phase-transfer photocatalytic process under ambient condition. We show that both photocatalytic reduction of O_2 and photocatalytic oxidation of H_2O are responsible for H_2O_2 production in this phase-transfer photocatalytic process, and the solvent permittivity and intermolecular interaction between O_2 and organophotocatalyst are the keys to achieve high efficiency. The photocatalytic H_2O_2 production rate in the system reaches 9000 μmol g^{-1} h^{-1} in the initial stage under ambient condition , and the apparent quantum efficiency (AQE) was ca. 8.2% based on the 595 nm wavelength. This work brings new insight to H_2O_2 production in a distinct mechanism that may inspire the development of low-energy consumption and cost-effective H_2O_2 production through photocatalysis.

1. Introduction

As one of the cleanest and most versatile chemicals, hydrogen peroxide (H_2O_2) has long been widely applied in chemical industry and environmental remediation [1–3]. After nearly a century of industrialization, the anthraquinone oxidation (AO), alcohol oxidation, and electrochemical synthesis have been figured out as practical ways for large-scale H_2O_2 production [4–8]. The AO process was introduced in 1940s, [9] which dominates 95% of H_2O_2 production worldwide merited by its high yield and safety that avoids the direct contact of H_2 and O_2. The AO processes [10] produce 1–2% (w/w) H_2O_2 solution which cost 17.6 kWh kg^{-1} energy on the hydrogenation step. The alcohols oxidation process [11–13] was introduced as early as 1957, which affords high H_2O_2 concentration (7.5%, w/w) and selectivity (97%) under high temperature and pressure (> 100 ℃, ca. 10 bar) with ketone compounds as coproduct. The electrochemical synthesis could be traced back to 1895, which can produce 2% (w/w) HO_2^- (1.6 V, 0 ℃). However, the utilization of the full potential of H_2O_2 needs alternative technologies based on clean and low cost [14–17].

Alternatively, H_2O_2 production from a photocatalytic process may provide an alternative solution to address the existing challenges by taking the advantages of unlimited natural resources such as water, air

* Corresponding authors.
** Corresponding author at: Institute of Functional Nano & Soft Materials (FUNSOM), Jiangsu Key Laboratory for Carbon-Based Functional Materials & Devices, Soochow University, 199 Ren'ai Road, Suzhou 215123, Jiangsu, China.
E-mail addresses: hplin@snnu.edu.cn (H. Lin), yuzhao@suda.edu.cn (Y. Zhao), zhkang@suda.edu.cn (Z. Kang).
[1] These authors contributed equally to this work.

https://doi.org/10.1016/j.apcatb.2022.121499
Received 11 January 2022; Received in revised form 16 April 2022; Accepted 8 May 2022
Available online 11 May 2022

and solar irradiation [18,19]. In this process, H_2O_2 can be produced via a two-electron process either through the reduction of O_2 or through the oxidation of H_2O with the assistance of proper photocatalysts [20,21]. Presently, photocatalytic H_2O_2 production is dominated by heterogeneous catalytic systems [22–24]. Shiraishi et al. have achieved H_2O_2 production by using a resorcinol-formaldehyde resin as metal-free photocatalyst with solar-to-chemical conversion efficiency of ca. 0.5% [25]. Our group has realized H_2O_2 production free of scavenger in O_2 saturated water by using ZIF-8/C_3N_4 composite powders as the photocatalyst [26]. As the only case in quasi-homogeneous catalytic system, Krivtsov et al. have demonstrate H_2O_2 production can be achieved by using soluble carbon nitride as the photocatalyst [27]. Nonetheless, challenges still remain for industrial production, such as (1) the catalyst should compatible with homogeneous system and easy to separate for continuous production, (2) the produced H_2O_2 should be stabilized and separated to avoid decomposition, and (3) the synthetic system should be simplified to lower down the cost and avoid the use of additional scavengers, vacuum condition and so forth.

We propose in this study an anthracene-derivative-catalyzed phase-transfer photocatalytic process for highly efficient H_2O_2 production and separation using H_2O and O_2 as the reactants. The phase-transfer photocatalytic process enables the extraction of formed H_2O_2 from the organic to the aqueous phase, while the separation process coupled with reaction process decreases the degradation of the formed H_2O_2 with the oxidation or disproportionation. The anthracene-derivative-based organophotocatalyst shows preferential chemisorption to O_2, and possesses proper electronic structure that is capable to produce H_2O_2 via photocatalytic reactions. Moreover, in-situ FTIR and transient photovoltage measurement (TPV) confirmed that the photocatalytic H_2O_2 production is as a result of both the reduction reaction of O_2 and the oxidation reaction of H_2O, during which the charge separation efficiency and the formation process of H_2O_2 can be controlled by tuning the permittivity of the organic solvent. As a result, the photocatalytic H_2O_2 production rate reaches 9000 μmol g^{-1} h^{-1} in the initial stage under ambient condition and AM 1.5 G illumination without using sacrificial agent or yielding by-products. It is the first demonstration of H_2O_2 production from the photocatalytic process using an organophotocatalyst and a phase-transfer homogeneous catalytic system.

2. Experimental

2.1. Synthesis of 9,10-Bis(4-trimethylsilylphenylethynyl)anthracene

As shown in Fig. S1, a solution of 9,10-dibromoanthracene (1.48 g, 5 mmol), trimethylsilylacetylene (1.96 g, 20 mmol), $Pd(PPh_3)_2Cl_2$ (360 mg, 0.48 mmol) and CuI (570 mg, 3 mmol) in dry diisopropyamine (20 mL) and dry THF (60 mL) was refluxed for 8 h. After cooling water (30 mL) was added and the mixture was extracted with dichloromethane (3 ×30 mL). The combined organic fractions were dried with sodium sulfate and the solvent was evaporated. Chromatography (hexane) afforded the product compound 1 as deep-red solid (1.83 g, 97% yield).

2.2. Synthesis of 9,10-Bis(ethynyl)anthracene

Compound 1 (1.48 g, 4.0 mmol) was dissolved in 30 mL THF and the solution was degassed for 15 min. Then KOH (448 mg, 8.0 mmol, in 18 mL methanol) was added via syringe. After TLC analysis showed that the starting material was completely consumed, CH_2Cl_2 (150 mL) was added. The solution was washed with water and dried over anhydrous Na_2SO_4. A brown solid was obtained as the product after removal of the solvents under vacuum (886 mg, 98%).

3. Results and discussion

3.1. The phase-transfer photocatalytic process

The phase-transfer photocatalytic process is schematically shown in Fig. 1. The synthetic system is designed by taking advantage of solubility difference of H_2O_2 and organophotocatalyst in two immiscible phases. Molecules with appropriate electronic structure that is suitable for photocatalytic reduction of O_2 and/or oxidation of H_2O may fulfill the role for H_2O_2 generation. Upon irradiation, H_2O_2 is in-situ produced in the organic phase either by the photo-excited electrons or holes from the photocatalyst through the reduction reaction of O_2 or the oxidation reaction of H_2O, respectively. Simultaneously, the produced H_2O_2 is immediately extracted and isolated by the aqueous phase to avoid decomposition. Considering that the solubility of H_2O_2 is much greater in the aqueous phase, the extraction of H_2O_2 from the organic phase is feasible.

3.2. Characterization of small-molecule catalyst

As a proof-of-concept study, an anthracene derivative, 9,10-bis(ethynyl)anthracene (DAn), was synthesized and used as the organophotocatalyst owing to the rigid molecular skeleton that make it almost insoluble in aqueous phase, and well-established modification method to tune the electronic properties. DAn was synthesized through Sonogashira reaction (Fig. 2a). ^{1}H NMR spectrum shown in Fig. 2b confirmed the as-prepared product was DAn, which turned out to be irregular particles with amorphous nature (Fig. S2). DAn powder showed strong absorption in the regions of visible and ultraviolet light, further extended to the near infrared region (Fig. 2c). The HOMO and LUMO was determined by cyclic voltammetry method to be 1.98 and − 1.00 V vs RHE, respectively, (Fig. 2d). DAn solution exhibited an onset wavelength of ca. 426 nm at room temperature (Fig. 2e), corresponding to a band gap of 2.91 eV. The HOMO of DAn was more positive than the potential of O_2 reduction, while the LUMO of DAn was more negative than the potential of H_2O oxidation (Fig. 2f). From a thermodynamic view, DAn is capable for the photocatalytic H_2O_2 production both by O_2 reduction and H_2O oxidation. In addition, it's found that the emission intensity of photoluminescence (PL) spectra of DAn solution increased in the solvent with higher permittivity. This is because increased solvent permittivity is beneficial to stabilize the excited state of DAn as a result of π-π * transition [28].

3.3. Photocatalytic properties

The DAn-catalyzed H_2O_2 production was evaluated in a customized phase-transfer photocatalytic system composed of 5 mg DAn, 5 mL dichloromethane (DCM) as the organic phase and 20 mL water as both the reactant and extractant under visible light irradiation without sacrificial agent. A H_2O_2 evolution rate of ca. 9000 μmol g^{-1} h^{-1} was achieved under ambient condition in the first half hour (Fig. 3a), and gradually stabilized at ca. 2434 μmol g^{-1} h^{-1} as the diffusion of O_2 across the air-water interface and the water-DCM interface establishing an equilibrium state. In replacing water to collect H_2O_2 every 12 h, and repeated the experiment five times. As shown in Fig. S3, after five cycles of photocatalytic reaction, the H_2O_2 formation rate still remains at 2243.48 μmol g^{-1} h^{-1}, indicating that DAn exhibits high stability in the phase-transfer photocatalytic system. Under O_2 atmosphere, the H_2O_2 evolution rate could be further boosted to 11,200 μmol g^{-1} in the first half hour and stabilized at ca. 3170 μmol g^{-1} h^{-1}. The H_2O_2 evolution rate increased under the O_2-saturated photocatalytic phase-transfer system, which illustrated that the H_2O_2 evolution rate is related to the O_2 reactant. The AQE was ca. 8.2% based on the 595 nm wavelength. (Fig. 3b and Table S1). The total H_2O_2 yield reached 210.2 and 162.5 μmol in O_2 atmosphere and air, respectively (Fig. 3c). Such a performance is superior to most state-of-the-art H_2O_2 production via the

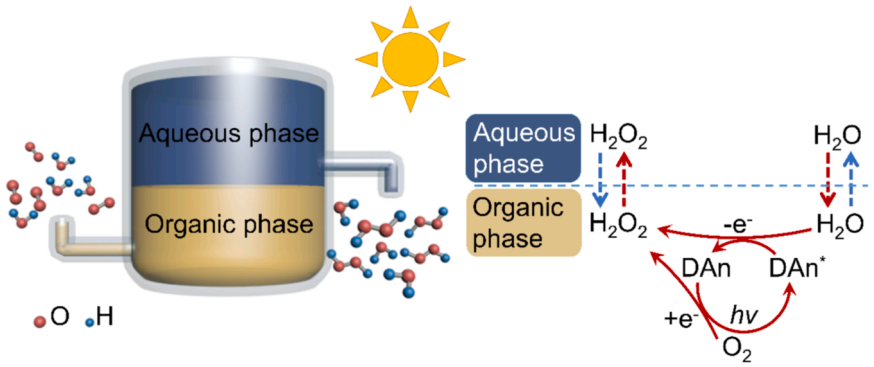

Fig. 1. Schematic illustration of the phase-transfer photocatalytic process for simultaneous H_2O_2 production and separation.

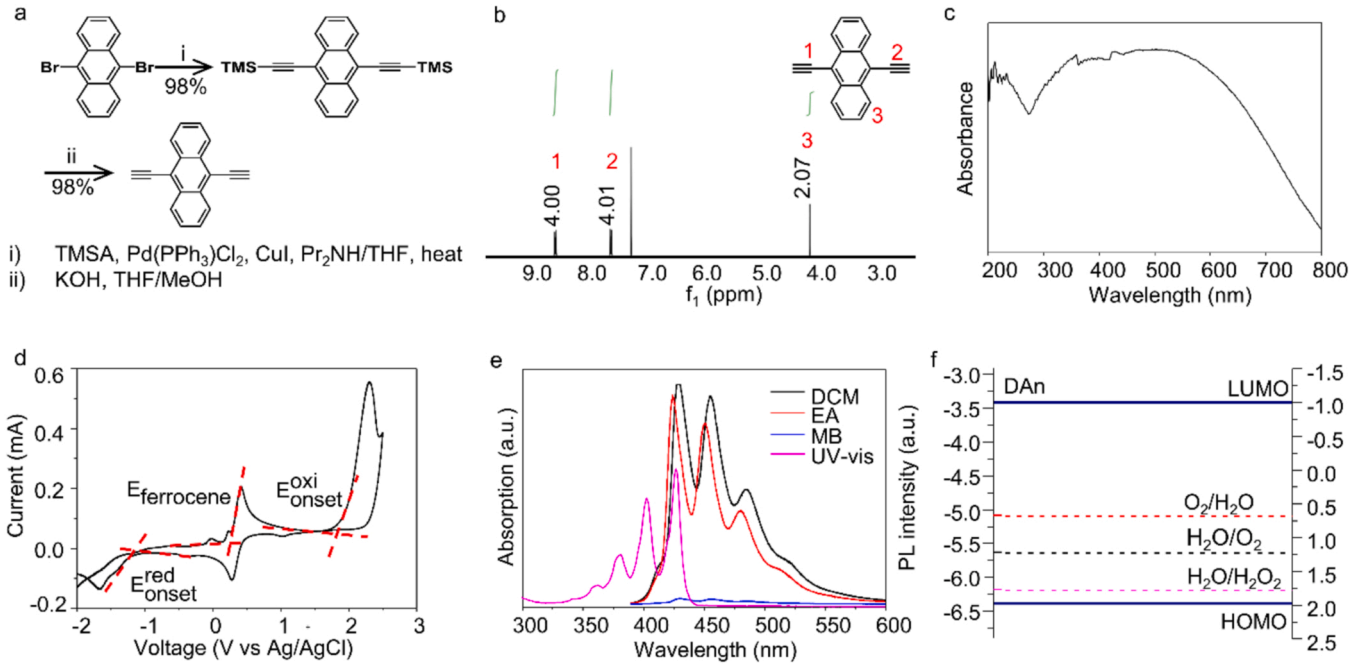

Fig. 2. Preparation and characterization of DAn organophotocatalyst. (a) Synthetic route, (b) ^{1}H NMR spectrum and (c) UV–vis spectrum of the as-prepared DAn powder. (d) CV profile, (e) UV–vis absorption and PL spectra of DAn solution. (f) Schematic of the HOMO/LUMO energy level with respect to the potentials of O_2 reduction and H_2O oxidation reactions.

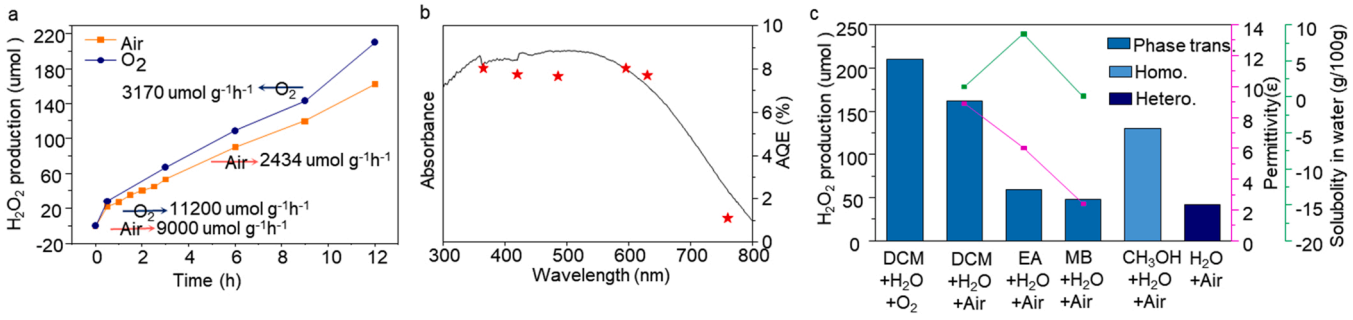

Fig. 3. H_2O_2 evolution rate in the phase-transfer photocatalytic process. (a) H_2O_2 evolution rate versus time. (b) UV–vis absorption spectra of the reactant solution and corresponding AQE in the phase-transfer photocatalytic process. (c) Comparison of total H_2O_2 evolution in various photocatalytic system.

photocatalytic process (Table S2). Moreover, DAn showed higher photocatalytic activity in the organic phase with higher permittivity. For instance, the total H_2O_2 yield was decreased to 58.8 and 48.0 μmol as the permittivity decreased from 8.9 (DCM) to 6.03 (ethyl acetate, EA) and 2.38 (methylbenzene, MB), respectively (pink curve, Fig. 3c). Such a difference in photocatalytic activity should be contributed from the difference of permittivity that higher permittivity is beneficial to stabilizing the excited state of DAn, rather than the water content in the organic phase because the water solubility in the organic phase did not follow a proportional relationship as indicated in the green curve of

Fig. 3c. In addition, the photocatalytic process showed lower total H_2O_2 yield without the phase-transfer process. For instance, the total H_2O_2 yield for homogeneous and heterogeneous photocatalytic processes was 130.0 and 41.5 μmol, respectively, corresponding to an increased yield of 25% and 292% after integration of the phase-transfer process that is beneficial for immediate H_2O_2 extraction to the aqueous phase to avoid decomposition and resultant equilibrium shift towards H_2O_2 production in the organic phase. Besides, it's found that the amount of H_2O_2 production showed linear relationship with the volume of the organic phase (Fig. S4), demonstrating that the DAn-catalyzed H_2O_2 production was more likely to occur in the organic phase rather than on the aqueous-organic interface [29].

3.4. Mechanism of the phase-transfer photocatalytic process

To further demonstrate the effect of solvent permittivity on the catalytic activity of DAn, in-situ TPV measurements were carried out to assess the charge transfer dynamics in the phase-transfer photocatalyst system. To mimic the chemical environment in the organic phase, DAn was filmed to an ITO substrate, then the organic solvent was nebulized and sprayed onto the DAn film to form a thin liquid layer (Fig. S5). A 355 nm pulse laser (5 ns) was used to excite the DAn while collecting the TPV signal simultaneously. The influence of solvent permittivity was verified by the in-situ TPV measurements under DCM, EA, and MB atmosphere respectively. Upon irradiation, the excited charges of DAn were transferred to the ITO substrate, and all the excited charges were collected on the ITO substrate and charge recombination due to the bulk and interfacial recombination could be identified. As shown in Fig. 4a, the extracted charges (ΔQ) were estimated by the integrated area (S) from the moment to collect the charges on the ITO surface (t_0) to the moment when the output voltage reaching a maximum value (t_{max}). The relaxation time constant (τ, Fig. 4b–d) could be fitted by exponential function responding to the recombination curves. The value of ΔQ and τ significantly enhanced with the increase of permittivity, demonstrating that permittivity of organic solvent can stabilize the excited state of DAn.

Theoretical calculations were performed with Gaussian 09 suite to reveal the mechanism [30]. The CAM-B3LYP exchange-correlation energy functional was employed to describe electron-electron interactions [31]. All structures were optimized with the 6–31G(d) basis set [32]. The solvent effect was simulated with self-consistent reaction field (SCRF) theory performed on the Polarizable Continuum Model (PCM) [33–35]. Considering that no sacrificial is require in catalysis, two possible reaction pathways are illustrated in Fig. 5a and b. The potential limiting step was the combination two adsorbed hydroxyl groups to produce a H_2O_2 molecule through both reaction mechanisms, Fig. 5c shows HOMO and LUMO of this structure, in which two hydroxyl groups are bonded with the acetenyl group of DAn. Of importance, the electronic states of LUMO exhibited a clear anti-bonding mode consisting well with the scission of C-OH bonds upon irradiation. The calculated HOMO-LUMO gap of this structure in is 2.62, 2.64 and 2.70 eV in DCM, EA, and MB, respectively. This reveals that the C-OH bond cleavage is more feasible in solutions with larger solvent permittivity. In addition, the Gibbs free energy of this structure is also lower with increasing permittivity of solvents, revealing that the permittivity of organic solutions may not only stabilize this structure, but also enhance the formation of H_2O_2.

Next, we show the chemisorption O_2 on DAn also played a key role in enhancing the photocatalytic activity. The charge generated by DAn with O_2-saturated liquid layer in the in-situ TPV test was apparently greater than that with N_2-saturated liquid layer (Fig. S6). This can be attributed to the strong adsorption of O_2 on DAn, which creates an interface with photo activity in the O_2-DAn complex, promoting the effective separation of photogenerated charges. The O_2 adsorption properties of DAn was also investigated by O_2/N_2 sorption isotherm and O_2 temperature programmed desorption (TPD). The O_2 adsorption on DAn increased linearly at 273 K with increased pressure and reached 0.15 mmol g^{-1} at 1.0 bar, higher than N_2 adsorption of 0.09 mmol g^{-1} (Fig. S7a), indicating DAn shows a tendency to preferentially adsorbs O_2. O_2 TPD curve (Fig. S7b) revealed two pronounced peaks that can be clearly observed in two temperature regions. The peak at 80–140 ℃ was attributed to the typical O_2 physisorption signal due to its low-temperature desorption, and the peak locates beyond 180 ℃ confirmed the O_2 desorption that confirming the chemisorption of O_2 on DAn [36–38].

In-situ FTIR was carried out to monitor the intermediates during the photocatalytic process. As shown in Fig. 6a, the absorbance band of vaporous water (centered at 3642 cm^{-1} and 1638 cm^{-1}) in the organic

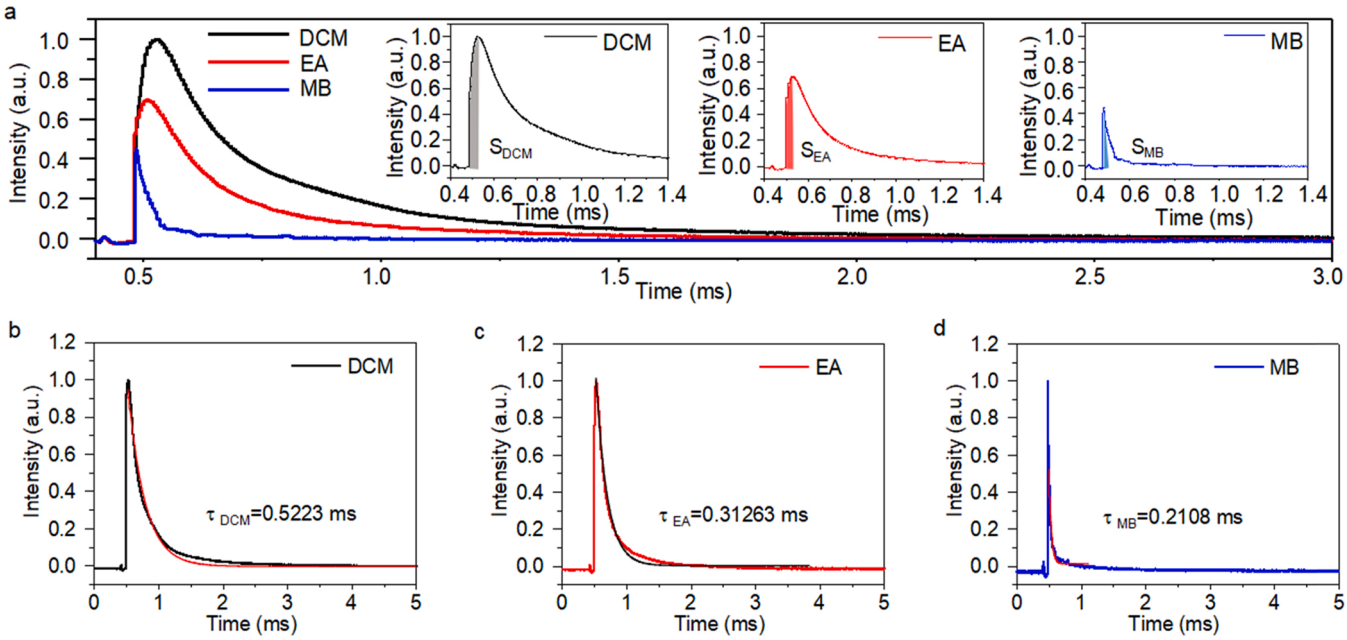

Fig. 4. Effect of solvent permittivity and O_2 chemisorption on the photocatalytic process. (a) TPV profiles with extracted charges (ΔQ) obtained under DCM, EA and MB atmosphere. Corresponding relaxation time constant (τ) obtained under DCM (b), EA (c) and MB (d).

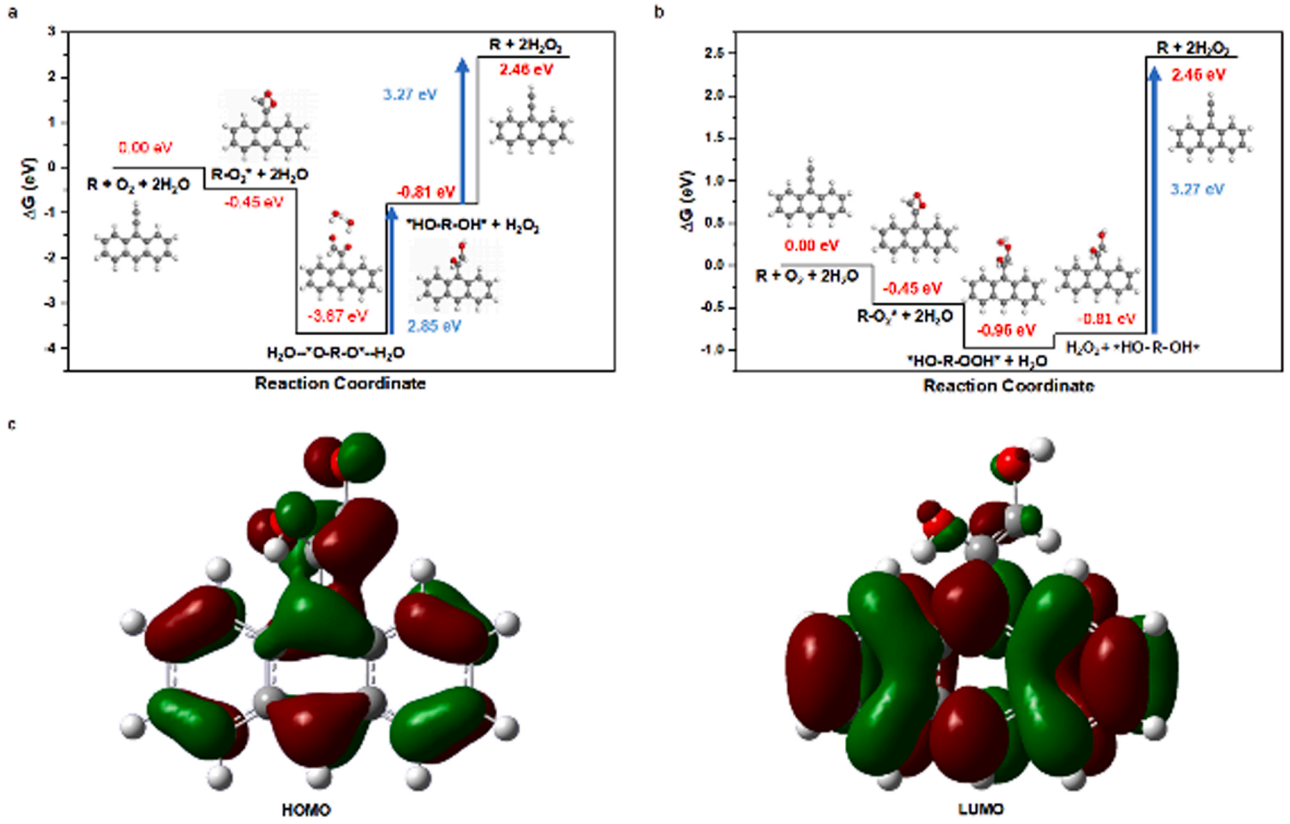

Fig. 5. The reaction path and energy diagram of H_2O_2 production catalyzed by DAn. (a) The synergistic mechanism involving the dissociation of two water molecules at the same time. (b) The dissociative mechanism involving the activation of one water molecule at each time. In both mechanisms, the potential limiting step is the breaking of two C-OH bonds and the subsequent combination of two OH to produce a H_2O_2 molecule. The carbon, oxygen and hydrogen atoms are represented with gray, red and white circles. (c)The highest occupied molecular orbital (HOMO) and lowest unoccupied molecular orbital (LUMO) of two hydroxyl group bonded to DAn. In the LUMO, the electronic states exhibit an anti-bonding mode, which consisting with the scission of C-OH bonds upon irradiation.

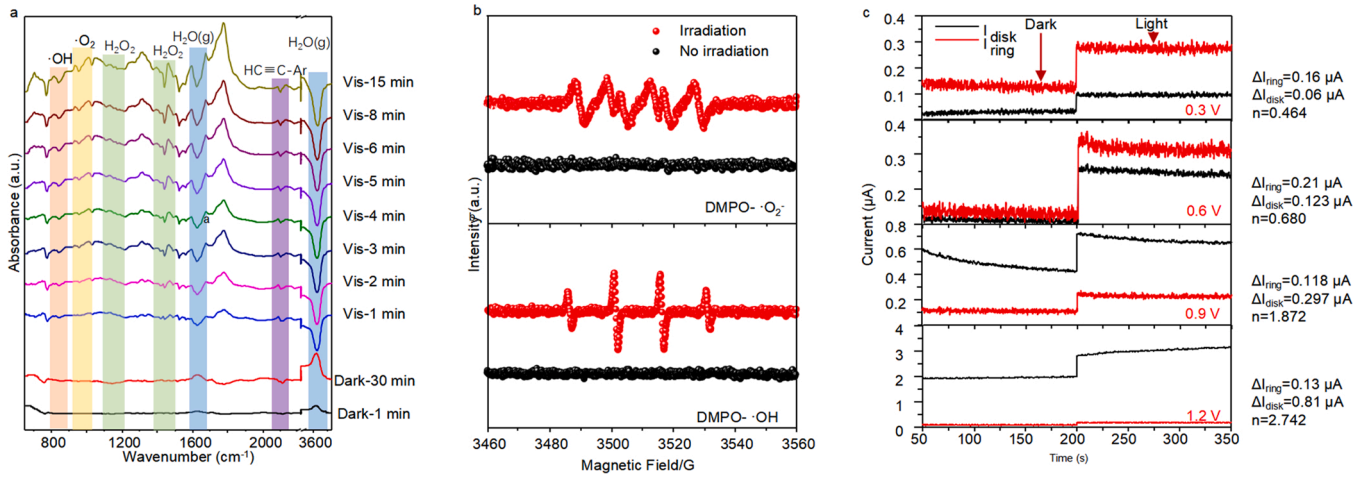

Fig. 6. Mechanism of H_2O_2 production during the photocatalytic process. (a) In-situ FTIR spectra of the organic phase upon irradiation at different time intervals. (b) DMPO spin-trapping EPR spectra showing the intermediates generated from the photocatalytic reduction of O_2 and oxidation of H_2O. (c) RRDE profiles recorded with and without irradiation at different potentials.

phase decreased upon prolonged irritation time, supposing that the water exhaustion could be either arise from the photocatalytic reduction of O_2 or the photocatalytic oxidation of H_2O. The former used water as the proton carrier, while the latter used water as the hole reactant [35]. Two new bands appeared at 813 cm^{-1} and 877 cm^{-1} (Fig. S8a), which can be assigned to the·OH radical generated through DAn*-induced oxidation reaction of water, and to the characteristic absorption band of H_2O_2, respectively [39]. Hence, DAn-catalyzed H_2O oxidation was a possible pathway for H_2O_2 production. On the other hand, the two new band located at 933 and 1011 cm^{-1} appeared after irradiation (Fig. S8b). The band at 933 cm^{-1} was due to O-O stretching of peroxide species ($\cdot O_2$), and the band at 1011 cm^{-1} was due to the protonated species, [40] confirming the existence of characteristic intermediates during O_2 reduction. Moreover, the new bands in the region of

1120–1200 cm^{-1} corresponding to OOH bending of free H_2O_2, and other bands at 1389 cm^{-1} (OH bending in H_2O_2) and 1460 cm^{-1} (*OOH) also supported the H_2O_2 production through O_2 reduction (Fig. S8c) [41]. In addition, DMPO spin-trapping electron paramagnetic resonance (EPR) spectra (Fig. 6b and c) also suggested the presence of $\cdot O_2^-$ and ·OH species during the photocatalytic process, which illustrate the dual-channel photocatalytic H_2O_2 production. Therefore, the photocatalytic process for H_2O_2 production could be regarded as a result of both DAn-mediated photocatalytic reduction of O_2 and photocatalytic oxidation of H_2O. During the photocatalytic process, DAn was found to be highly stable, no sign of degradation was observed (Fig. S9).

The electron transfer number during the H_2O oxidation process was determined by rotating ring-disk electrode (RRDE). The experimental setup was shown in Fig. S10. The electrode was composed of a disk DAn-coated glassy carbon electrode and a Pt ring electrode. Under open circuit voltage without O_2, the former was used to detect the photocurrent generated from the oxidation of H_2O, which leads to either the formation of H_2O_2 via a two-electron pathway or O_2 via a four-electron pathway, [42,43] while the latter corresponded to the current of electrochemical oxidation of the generated H_2O_2 under 0.9 V vs. NHE. Once H_2O_2 formed under irradiation on the DAn-disk electrode, the current change resulted from the oxidation of H_2O_2 could be detected by the Pt-ring electrode. While, if O_2 was produced on the DAn-disk electrode under irradiation, there would be no obvious current change on the Pt-ring electrode. The RRDE profiles were shown in Fig. 6c. The calculated electron transfer number was 0.464 under open circuit voltage, and 0.680, 1.87 and 2.742 under 0.6, 0.9 and 1.2 V vs. NHE (Table S3), in which, it is smaller than the ideal value of 2 under open circuit voltage [26]. These results further confirm the strong chemisorption of O_2 on DAn and the photo activity nature of the O_2-DAn complex, as the DAn-disk electrode must apply a more positive voltage to exclude the interference of the cathodic current from O_2 reduction [44]. Above all, the equations describing the full pathway for H_2O_2 in the phase-transfer and heterogeneous photocatalytic system were summarized as follows:

Phase-transfer photocatalysis:

$$R + O_2 \rightarrow R - O_2* \rightarrow H_2O - *O - R - O* \xrightarrow{-H_2O} \xrightarrow{+2e^-} *HO - R - OH$$

$$* + H_2O_2 \xrightarrow{+2e^-} R + 2H_2O_2$$

Heterogeneous photocatalysis:

$$R + O_2 \xrightarrow{+e^-} R - O_2^- \xrightarrow{+e^-} R - O_2^{2-} \xrightarrow{+H^+} R - O_2H^- \xrightarrow{+H^+} R + H_2O_2$$

$$R + 2H_2O \xrightarrow{+H^+} H_2O_2 + 2H^+$$

4. Conclusion

In summary, we propose a DAn-catalyzed, phase-transfer photocatalytic process towards highly efficient H_2O_2 production. This method can be operated under ambient condition and avoids the use of additional scavengers. The DAn organophotocatalyst exhibits strong chemisorption to O_2, possesses proper electronic structure towards O_2 reduction and H_2O oxidation, and can be stabilized by tuning the permittivity of the solvent. As a result, the H_2O_2 evolution rate under ambient condition reaches ca. 9000 and 2434 μmol g^{-1} h^{-1} in the early stage and through the whole photocatalytic process, respectively. Combined with in-situ FTIR and TPV analysis, such a high efficiency is attributed to the phase-transfer system that is highly effective for in-situ generation of H_2O_2 and simultaneous extraction of the generated H_2O_2 from the organic phase to the aqueous phase to avoid further decomposition, and the photocatalytic process that features both O_2 reduction reaction and H_2O oxidation reaction for H_2O_2 production. The DAn-catalyzed phase-transfer photocatalytic process overcomes the challenges from conventional methods such as high-energy consumption synthesis and the use of additional scavengers, and features the possibility for continuous H_2O_2 production without further purification and catalyst recycling from the heterogeneous catalytic system, thus providing a highly promising alternative for H_2O_2 production with high efficiency and low cost.

CRediT authorship contribution statement

Yu Zhao: Data curation, Visualization. **Xinke Li:** Investigation. **Xing Fan:** Formal analysis. **Hongshuai Wang:** Investigation, Software. **Yunliang Liu:** Software. **Yuanyuan Chen:** Investigation. **Tianyu Yang:** Investigation. **Jing Ye:** Investigation. **Hui Huang:** Writing – original draft, Project administration. **Haitao Li:** Investigation. **Xiaohong Zhang:** Project administration. **Yang Liu:** Resources, Writing – review & editing, Supervision. **Haiping Lin:** Writing – review & editing, Supervision. **Yu Zhao:** Writing – review & editing, Supervision. **Zhenhui Kang:** Conceptualization, Funding acquisition, Writing – review & editing, Supervision.

Declaration of Competing Interest

The authors declare no conflict of interest.

Acknowledgements

This work is supported by the National Key Research and Development Project of China (2020YFA0406101, 2020YFA0406104, 2020YFA0406103), National MCF Energy R&D Program (2018YFE0306105), National Natural Science Foundation of China (22179031, 51725204, 21771132, 51972216, 52041202), Innovative Research Group Project of the National Natural Science Foundation of China (51821002), Natural Science Foundation of Jiangsu Province (BK20190041), Key-Area Research and Development Program of GuangDong Province (2019B010933001), Collaborative Innovation Center of Suzhou Nano Science & Technology, the 111 Project and Suzhou Key Laboratory of Functional Nano & Soft Materials.

Appendix A. Supporting information

Supplementary data associated with this article can be found in the online version at doi:10.1016/j.apcatb.2022.121499.

References

[1] R. Hage, A. Lienke, A, Applications of transition-metal catalysts to textile and wood-pulp bleaching, Angew. Chem. Int. Ed. 45 (2006) 206–222, https://doi.org/10.1002/anie.200500525.
[2] L. Zhou, J. Feng, B. Qiu, Y. Zhou, J. Lei, M. Xing, L. Wang, Y. Zhou, Y. Liu, J. Zhang, Ultrathin g-C_3N_4 nanosheet with hierarchical pores and desirable energy band for highly efficient H_2O_2 production, Appl. Catal. B Environ. 267 (2020), 118396, https://doi.org/10.1016/j.apcatb.2019.118396.
[3] C. Feng, L. Tang, Y. Deng, J. Wang, Y. Liu, X. Ouyang, H. Yang, J. Yu, J. Wang, A novel sulfur-assisted annealing method of g-C_3N_4 nanosheet compensates for the loss of light absorption with further promoted charge transfer for photocatalytic production of H_2 and H_2O_2, Appl. Catal. B Environ. 281 (2021), 119539, https://doi.org/10.1016/j.apcatb.2020.119539.
[4] J.M. Campos-Martin, G. Blanco-Brieva, J.L. Fierro, Hydrogen peroxide synthesis: an outlook beyond the anthraquinone process, Angew. Chem. Int. Ed. 45 (2006) 6962–6984, https://doi.org/10.1002/anie.200503779.
[5] Y. Hou, Y. Wang, F. He, S. Han, Z. Mi, W. Wu, E. Min, Liquid phase hydrogenation of 2-ethylanthraquinone over La-doped Ni–B amorphous alloy catalysts, Matt. Lett. 58 (2004) 1267–1271, https://doi.org/10.1016/j.matlet.2003.09.019.
[6] R. Dittmeyer, J.-D. Grunwaldt, A. Pashkova, A review of catalyst performance and novel reaction engineering concepts in direct synthesis of hydrogen peroxide, Catal. Today 248 (2015) 149–159, https://doi.org/10.1016/j.cattod.2014.03.055.
[7] J. Tan, Z.D. Liu, Y.C. Lu, J.H. Xu, G.S. Luo, Process intensification of H_2O_2 extraction using gas–liquid–liquid microdispersion system, Sep. Purif. Technol. 80 (2011) 225–234, https://doi.org/10.1016/j.seppur.2011.04.030.
[8] K.D. Samant, K.M. Ng, Synthesis of extractive reaction processes, AIChE J. 44 (1998) 1363–1381, https://doi.org/10.1002/aic.690440615.
[9] H.-J. Riedl, G. Pfleiderer, (I. G. Farbenindustrie AG.), US 2158525,1939 [Chem. Abstr., 1939, 33, 49337].
[10] A.T. Murray, S. Voskian, M. Schreier, T.A. Hatton, Y. Surendranath, Electrosynthesis of hydrogen peroxide by phase-transfer catalysis, Joule 3 (2019) 2942–2954, https://doi.org/10.1016/j.joule.2019.09.019.

[11] D.G. Hendry, G.A. Russell, Solvent effects in the reactions of free radicals and atoms. IX. Effect of solvent polarity on the reactions of peroxy radicals, J. Am. Chem. Soc. 86 (1964) 2368–2371, https://doi.org/10.1021/ja01066a014.
[12] G.A. Russell, The rates of oxidation of aralkyl hydrocarbons. Polar effects in free radical reactions[1, 2], J. Am. Chem. Soc. 78 (1956) 1047–1054, https://doi.org/10.1021/ja01586a047.
[13] C.R. Harris. (E. I. Du Pont de Nemours and Company), US 2479111, 1949 [Chem. Abstr.,1949, 44, 5600].
[14] Z. Haider, H. Cho, G. Moon, H. Kim, Minireview: Selective production of hydrogen peroxide as a clean oxidant over structurally tailored carbon nitride photocatalysts, Catal. Today 335 (2019) 55–64, https://doi.org/10.1016/j.cattod.2018.11.067.
[15] C. Xia, Y. Xia, P. Zhu, L. Fan, H. Wang, Direct electrosynthesis of pure aqueous H_2O_2 solutions up to 20% by weight using a solid electrolyte, Science 366 (2019) 226–231, https://doi.org/10.1126/science.aay1844.
[16] Z. Lu, G. Chen, S. Siahrostami, Z. Chen, Y. Cui, High-efficiency oxygen reduction to hydrogen peroxide catalysed by oxidized carbon materials, Nat. Catal. 1 (2018) 156–162, https://doi.org/10.1038/s41929-017-0017-x.
[17] C. Xia, J.Y. Kim, H. Wang, Recommended practice to report selectivity in electrochemical synthesis of H_2O_2, Nat. Catal. 3 (2020) 605–607, https://doi.org/10.1038/s41929-020-0486-1.
[18] Y. Yang, G. Zeng, D. Huang, C. Zhang, D. He, C. Zhou, W. Wang, W. Xiong, X. Li, B. Li, W. Dong, Y. Zhou, Molecular engineering of polymeric carbon nitride for highly efficient photocatalytic oxytetracycline degradation and H_2O_2 production, Appl. Catal. B Environ. 272 (2020), 118970, https://doi.org/10.1016/j.apcatb.2020.118970.
[19] J. Zhang, J. Lang, Y. Wei, Q. Zheng, L. Liu, Y. Hu, B. Zhou, C. Yuan, M. Long, Efficient photocatalytic H_2O_2 production from oxygen and pure water over graphitic carbon nitride decorated by oxidative red phosphorus, Appl. Catal. B Environ. 298 (2021), 120522, https://doi.org/10.1016/j.apcatb.2021.120522.
[20] J.J. Cao, Q. Wu, Y. Zhao, K. Wei, Y. Li, X. Wang, F. Liao, H. Huang, Y. Liu, Z. Kang, In-situ photovoltage transients assisted catalytic study on H_2O_2 photoproduction over organic molecules modified carbon nitride photocatalyst, Appl. Catal. B Environ. 285 (2021), 119817, https://doi.org/10.1016/j.apcatb.2020.119817.
[21] J. Liu, Y. Liu, N. Liu, Y. Han, X. Zhang, H. Huang, Y. Lifshitz, S.-T. Lee, J. Zhong, Z. Kang, Metal-free efficient photocatalyst for stable visible water splitting via a two-electron pathway, Science 347 (2015) 970–974, https://doi.org/10.1126/science.aaa3145.
[22] Y. Liu, Y. Zhao, Y. Sun, J. Cao, H. Wang, X. Wang, H. Huang, M. Shao, Y. Liu, Z. Kang, A $4e^-$-$2e^-$ cascaded pathway for highly efficient production of H_2 and H_2O_2 from water photo-splitting at normal pressure, Appl. Catal. B Environ. 270 (2020), 118875, https://doi.org/10.1016/j.apcatb.2020.118875.
[23] S. Samanta, R. Yadav, A. Kumar, A.K. Sinha, R. Srivastava, Surface modified C, O co-doped polymeric g-C_3N_4 as an efficient photocatalyst for visible light assisted CO_2 reduction and H_2O_2 production, Appl. Catal. B Environ. 259 (2019), 118054, https://doi.org/10.1016/j.apcatb.2019.118054.
[24] J. Zhang, C. Yu, J. Lang, Y. Zhou, B. Zhou, Y. Hu, M. Long, Modulation of Lewis acidic-basic sites for efficient photocatalytic H_2O_2 production over potassium intercalated tri-s-triazine materials, Appl. Catal. B Environ. 277 (2020), 119225, https://doi.org/10.1016/j.apcatb.2020.119225.
[25] Y. Shiraishi, T. Takii, T. Hagi, S. Mori, Y. Kofuji, Y. Kitagawa, S. Tanaka, S. Ichikawa, T. Hirai, Resorcinol–formaldehyde resins as metal-free semiconductor photocatalysts for solar-to-hydrogen peroxide energy conversion, Nat. Mater. 18 (2019) 985–993, https://doi.org/10.1038/s41563-019-0398-0.
[26] Y. Zhao, Y. Liu, J. Cao, H. Wang, M. Shao, H. Huang, Y. Liu, H. Kang, Efficient production of H_2O_2 via two-channel pathway over ZIF-8/C_3N_4 composite photocatalyst without any sacrificial agent, Appl. Catal. B Environ. 278 (2020), 119289, https://doi.org/10.1016/j.apcatb.2020.119289.
[27] I. Krivtsov, D. Mitoraj, C. Adler, M. Ilkaeva, M. Sardo, L. Mafra, C. Neumann, A. Turchanin, C. Li, B. Dietzek, R. Leiter, J. Biskupek, U. Kaiser, C. Im, B. Kirchhoff, T. Jacob, R. Beranek, Water-soluble polymeric carbon nitride colloidal nanoparticles for highly selective quasi-homogeneous photocatalysis, Angew. Chem. Int. Ed. 59 (2020) 487–495, https://doi.org/10.1002/anie.201913331.
[28] H. Naito, K. Nishino, Y. Morisaki, K. Tanaka, Y. Chujo, Solid-state emission of the anthracene-*o*-carborane dyad from the twisted-intramolecular charge transfer in the crystalline state, Angew. Chem. Int. Ed. 56 (2017) 254–259, https://doi.org/10.1002/anie.201609656.
[29] G. Roagna, D.M.H. Ascough, F. Ibba, A.C. Vicini, A. Fontana, K.E.C. Peschiulli A., D. Oehlrich, A. Misale, A.A. Trabanco, R.S. Paton, G. Pupo, V. Gouverneur, Hydrogen bonding phase-transfer catalysis with ionic reactants: enantioselective synthesis of γ-fluoroamines, J. Am. Chem. Soc. 142 (2020) 14045–14051, https://doi.org/10.1021/jacs.0c05131.
[30] M.J. Frisch, G.W. Trucks, H.B. Schlegel, G.E. Scuseria, M.A. Robb, J.R. Cheeseman, J.V. Ortiz, gaussian 09, Revision d. 01, 201, Gaussian. Inc., Wallingford CT, 2009.
[31] T. Yanai, D.P. Tew, N.C. Handy, A new hybrid exchange–correlation functional using the Coulomb-attenuating method (CAM-B3LYP), Chem. Phys. Lett. 393 (2004) 51–57, https://doi.org/10.1016/j.cplett.2004.06.011.
[32] M.J. Frisch, J.A. Pople, J.S. Binkley, Self-consistent molecular orbital methods 25. Supplementary functions for Gaussian basis sets, J. Chem. Phys. 80 (1984) 3265–3269, https://doi.org/10.1063/1.447079.
[33] S. Miertuš, E. Scrocco, J. Tomasi, Electrostatic interaction of a solute with a continuum. A direct utilizaion of AB initio molecular potentials for the prevision of solvent effects, Chem. Phys. 55 (1981) 117–129, https://doi.org/10.1016/0301-0104(81)85090-2.
[34] S. Miertuš, J. Tomasi, Approximate evaluations of the electrostatic free energy and internal energy changes in solution processes, Chem. Phys. 65 (1982) 239–245, https://doi.org/10.1016/0301-0104(82)85072-6.
[35] J. Tomasi, M. Persico, Molecular interactions in solution: an overview of methods based on continuous distributions of the solvent, Chem. Rev. 94 (1994) 2027–2094, https://doi.org/10.1021/cr00031a013.
[36] R. Matsuda, R. Kitaura, S. Kitagawa, Y. Kubota, R.V. Belosludov, T.C. Kobayashi, H. Sakamoto, T. Chiba, M. Takata, Y. Kawazoe, Y. Mita, Highly controlled acetylene accommodation in a metal-organic microporous material, Nature 436 (2005) 238–241, https://doi.org/10.1038/nature03852.
[37] Y. Bai, L. Ye, T. Chen, P. Wang, L. Wang, X. Shi, P.K. Wong, Synthesis of hierarchical bismuth-rich $Bi_4O_5Br_xI_{2-x}$ solid solutions for enhanced photocatalytic activities of CO_2 conversion and Cr (VI) reduction under visible light, Appl. Catal. B Environ. 203 (2017) 633–640, https://doi.org/10.1016/j.apcatb.2016.10.066.
[38] Q. Wu, Q. Liu, Y. Zhou, Y. Sun, J. Zhao, Y. Liu, F. Liu, M. Nie, F. Ning, N. Yang, X. Jiang, X. Zhou, J. Zhong, Z. Kang, Carbon defect-induced reversible carbon–oxygen interfaces for efficient oxygen reduction, ACS Appl. Mater. Interfaces 10 (2018) 39735–39744, https://doi.org/10.1021/acsami.8b14323.
[39] R. Nakamura, A. Imanishi, K. Murakoshi, Y. Nakato, In situ FTIR studies of primary intermediates of photocatalytic reactions on nanocrystalline TiO_2 films in contact with aqueous solutions, J. Am. Chem. Soc. 125 (2003) 7443–7450, https://doi.org/10.1021/ja029503q.
[40] R. Nakamura, Y. Nakato, Primary intermediates of oxygen photoevolution reaction on TiO_2 (Rutile) particles, revealed by in situ FTIR absorption and photoluminescence measurements, J. Am. Chem. Soc. 126 (2004) 1290–1298, https://doi.org/10.1021/ja0388764.
[41] H. Li, H. Shang, X. Cao, Z. Yang, Z. Ai, L. Zhang, Oxygen vacancies mediated complete visible light NO oxidation via side-on bridging superoxide radicals, Environ. Sci. Technol. 52 (2018) 8659–8665, https://doi.org/10.1021/acs.est.8b01849.
[42] H. Li, P. Wen, D.S. Itanze, Z.D. Hood, S. Adhikari, C. Lu, X. Ma, C. Dun, L. Jiang, D. L. Carroll, Y. Qiu, S.M. Geyer, Scalable neutral H_2O_2 electrosynthesis by platinum diphosphide nanocrystals by regulating oxygen reduction reaction pathways. Nat. Commun. 11 (2020) 1–12, https://doi.org/10.1038/s41467-020-17584-9.
[43] C.M. Sánchez-Sánchez, A.J. Bard, Hydrogen peroxide production in the oxygen reduction reaction at different electrocatalysts as quantified by scanning electrochemical microscopy, Anal. Chem. 81 (2009) 8094–8100. ⟨https://doi.org/10.1021/ac901291v⟩.
[44] Q. Wu, M. Zhu, J. Cao, X. Wang, Y. Liu, C. Xiang, M. Shao, H. Tian, Z. Kang, Metal-free catalyst with large carbon defects for efficient direct overall water splitting in air at room pressure, ACS Appl. Mater. Interfaces 12 (2020) 30280–30288, https://doi.org/10.1021/acsami.0c02544.